Sodium channel Nav1.2-L1342P variant displaying complex biophysical properties renders hyperexcitability of cortical neurons derived from human iPSCs

Zhefu Que&[1,2], Maria I. Olivero-Acosta&[1,2], Jingliang Zhang [1,2], Muriel Eaton [1,2], William C. Skarnes[3], and Yang Yang[1,2*]

[1]Department of Medicinal Chemistry and Molecular Pharmacology, College of Pharmacy, Purdue University; [2]Purdue Institute for Integrative Neuroscience; [3]Cellular Engineering, The Jackson Laboratory for Genomic Medicine. &, equal contribution.

Keywords: voltage-gated sodium channel, micro-electrode array (MEA), electrophysiology, hyperexcitability, epilepsy, SCN2A, Nav1.2, L1342P variant on Nav1.2

* To whom correspondence should be addressed: Yang Yang, Ph.D.; Department of Medicinal Chemistry and Molecular Pharmacology, College of Pharmacy, Purdue University, Hall for Discovery and Learning Research (DLR), 207 S Martin Jischke Dr, West Lafayette, IN 47907, Tel: 765-494-2926, Fax: 765-494-1414, E-mail: yangyang@purdue.edu

Acknowledgments: The authors gratefully acknowledge support from the Purdue University Institute for Drug Discovery and Institute for Integrative Neuroscience. Y.Y. is supported by funds from Ralph W. and Grace M. Showalter Research Trust, and Purdue Big Idea Challenge 2.0 on Autism. M.I.O.A. is supported by Fulbright scholarship program. Yang lab is grateful to the *FamilieSCN2A* foundation for the Action Potential Grant support. We thank Dr. Amy Brewster for critical reading of this paper. This project was also funded, in part, with support from the Indiana Clinical and Translational Sciences Institute funded, in part by Award Number UL1TR002529 from the National Institutes of Health, National Center for Advancing Translational Sciences, Clinical and Translational Sciences Award.

Abstract:

With wide adoption of whole-exome sequencing in children with seizures, an increasing number of *SCN2A* variants has been revealed as genetic causes of epilepsy. Voltage-gated sodium channel Nav1.2, encoded by gene *SCN2A*, is strongly expressed in the pyramidal excitatory neurons and supports action potential firing. One recurrent *SCN2A* variant is L1342P, which was identified in multiple patients with early-onset encephalopathy and intractable seizures. Despite its recurrence, how this variant affects the functions of human neurons causing severe epileptic symptoms is largely elusive. To understand the core phenotype of the L1342P variant in human neurons, here we took advantage of a reference human induced pluripotent stem cell (hiPSC) line, in which L1342P was engineered by CRISPR/Cas9 mediated genome editing. Using patch-clamping and micro-electrode array (MEA) recording, we found that the cortical neurons derived from hiPSCs engineered with heterozygous L1342P variant have increased intrinsic excitability, higher current density, and enhanced synchronous network firing and bursting, showing a strong hyperexcitability phenotype. We further demonstrated that the L1342P neuronal culture has a degree of resistance to the anti-seizure medication (phenytoin), likely recapitulating aspects of clinical observation of patients carrying the L1342P variant. We further studied the efficacy of a Nav1.2 specific blocker Phrixotoxin-3 (PTx-3), which showed strong potency in reducing spontaneous and chemically induced excitability of neurons with the L1342P variant. Our results reveal a possible pathogenic mechanism underlying L1342P mediated seizures, and demonstrate the utility of genome-edited hiPSCs as *in vitro* platform to advance personalized phenotyping and drug discovery.

Introduction:

Epilepsy is a devastating neurological disease characterized by recurrent episodes of seizures, resulting from hypersynchronous firing of hyperexcitable neurons that go awry (Jiruska *et al.*, 2013). Affecting about 50 million people worldwide (WHO, 2019), its etiology can vary and can be caused by gene mutations (Shorvon, 2011). With the broad adoption of whole-exome sequencing in children with seizures, genetic variants in *SCN2A* have been increasingly identified, emerging as one of the leading genetic causes of epilepsies. *SCN2A*, encoding for the α-subunit of the voltage-gated sodium channel Nav1.2, is strongly expressed in many principal neurons of the central nervous system including excitatory neurons of the cortex (Hu *et al.*, 2009; Liao *et al.*, 2010; Tian *et al.*, 2014; Ye *et al.*, 2018). *SCN2A* is responsible for action potential (AP) initiation, propagation, and backpropagation in neurons during different developmental stages (Rush *et al.*, 2005) (Spratt *et al.*, 2019). Studies have found "hot spots" in *SCN2A*, where the variant occurs frequently. One of the leading recurrent Nav1.2 variants is L1342P. A heterozygous variant of L1342P has been reported in five patients identified from several different genetic studies, sharing similar and distinct features including early-onset epileptic encephalopathy, transient choreoathetotic movements, hypersomnia, among others (Matalon *et al.*, 2014; Dimassi *et al.*, 2016; Li *et al.*, 2016; Wolff *et al.*, 2017) (Hackenberg *et al.*, 2014). Most of these patients have intractable epilepsy and are resistant to the current medical treatment, which severely impairs their quality of life.

The channel properties of the L1342P variant have been previously studied in HEK293 cells, revealing profound alterations in gating properties and a mixed gain-loss of function phenotype (Begemann *et al.*, 2019). However, how L1342P variant affects the function of human neurons is largely unknown. Technology advance has made the generation of neurons from human-induced pluripotent stem cells (hiPSCs) possible, enabling the study of pathological features of human neurons *in vitro*. While patient-derived hiPSCs are often used for disease modeling, the genetic background of each patient may contribute to the phenotypes independent of the specific genetic mutation of interest, confounding the interpretation of experimental results. Additionally, when a variant affects more than one patient resulting in different clinical manifestations, it would be important to understand the core phenotypes that can be clearly attributed to the particular variant of interest. To this end, we employed a CRISPR/Cas9 mediated genome editing tool to generate the L1342P variant in a reference hiPSC (KOLF2) line. This particular line has a publicly available genome-sequencing, is highly accessible for cross-lab comparison, and demonstrated differentiation capacity into neurons (Skarnes *et al.*, 2019) (Leha *et al.*, 2016) (Streeter *et al.*, 2017).

By directly comparing neurons carrying Nav1.2-L1342P variant with their isogenic controls, here we report that the reference hiPSCs based *in vitro* model clearly show L1342P variant results in hyperexcitability phenotypes in neurons. Importantly, our *in vitro* platform is able to recapitulate aspects of pharmaco-responsiveness of patients, which may help to develop personalized therapy for epilepsy patients carrying specific genetic variants of *SCN2A*.

Results:

1. L1342P variant in Nav1.2 shows complex biophysical properties.

The α-subunit of Nav1.2 is composed of four homologous domains (I to IV), with each domain contains six transmembrane spanning regions (S1-S6). S1-S4 forms a voltage sensor domain (VSD), and S5-S6 helix with ion selectivity filter forms the pore domain, which permits sodium influx (**Figure 1A**). To visualize the location of the L1342P variant, we utilized a 3D human Nav1.2 structural model (6J8E) (**Figure 1B**) (Pan *et al.*, 2019). L1342P is positioned at the fifth segment (S5) on domain III, which is a highly conserved region (Begemann *et al.*, 2019). The fifth segment and neighboring locations are the hotspots for many seizure-related mutations (Sanders *et al.*, 2018). L1342P is also predicted to disturb interactions with the adjacent S4-S5 linker (Begemann *et al.*, 2019). The structural significance of the S5 region implies that the biophysical properties of Nav1.2 are likely to be profoundly disrupted by the L1342P variant.

To examine the effect of the L1342P variant on the biophysical properties of ion channels, we performed whole-cell voltage-clamp recordings on human embryonal kidney (HEK) cells transfected with expressing either wild-type (WT) or Nav1.2-L1342P mutant channel. Two representative whole-cell current traces from cells expressing either WT or Nav1.2-L1342P are shown, indicating that functional sodium currents can be recorded from both WT and Nav1.2-L1342P channels (**Figure 1C)**. The L1342P exhibited a large hyperpolarized shift of V_{half} in voltage-dependent activation compared to wild-type, suggesting a gain-of-function phenotype (**Figure 1D**) (V_{half} value: WT: –19.5 ± 0.5 mV, n = 9; L1342P: –35.4 ± 0.5 mV, n = 11; $p < 0.001$, *student's t-test*). Steady-state fast-inactivation was assessed in response to a 500 ms depolarizing potential. L1342P markedly shifted channel fast-inactivation V_{half} by around 16 mV in a depolarizing direction (**Figure 1E**) (V_{half} value: WT: –61.6 ± 0.1 mV, n = 6; L1342P: –77.8 ± 0.3 mV, n = 11; $p < 0.001$, *student's t-test*), suggesting a loss-of-function attribute. Taking channel activation and fast-inactivation together, the L1342P variant resulted in a complex biophysical change at the channel level, showing both gain and loss-of-function phenotypes for different parameters. To further understand the overall effect of these biophysical changes, we used the window current to determine the net effect of altered activation and inactivation of the L1342P variant. Window current is defined as the inward current that arises from partial activation and incomplete inactivation of the sodium channel (Patlak, 1991; Berecki *et al.*, 2018), which has been suggested to contribute to a persistent current affecting neuronal excitability (Taddese and Bean, 2002). The magnitude of window current can be used to assess the net effect of gain- v.s. loss-of-function of a particular variant. We calculated the window current of the WT channel as well as L1342P (**Figure 1F-G**), and found that the magnitude of the window current from L1342P is greater than that from WT (WT: INa/total = 5.8%; L1342P: INa/total = 7.0%). This enhanced window current is likely to contribute to an overall gain-of-function phenotype of the L1342P variant.

2. Single-compartmental simulation predicts a gain-of-function phenotype in a pyramidal neuron model with Nav1.2-L1342P variant.

To further study how the L1342P variant of Nav1.2 alters neuronal excitability, we used the NEURON simulation to model the firing properties of pyramidal neurons, in

which Nav1.2 is strongly expressed (Hu *et al.*, 2009; Liao *et al.*, 2010; Tian *et al.*, 2014; Ye *et al.*, 2018). We used the biophysical properties of WT and L132P Nav1.2 we measured in HEK cells as modeling parameters. We found that the neuron modeled with Nav1.2-L1342P is notably more excitable. Representative action potential firings in response to 1X to 5X current injection are shown (**Figure 2A)**, with 1X as the minimum current required to elicit an action potential in the L1342P neuron model. While neurons modeled with the L1342P variant started to fire action potential at 1X current injection, the same current injection cannot trigger action potential firing in neurons modeled with WT Nav1.2 channel (**Figure 2A)**. Action potential number of neurons modeled with Nav1.2-L1342P increases in response to elevated current injection and at each current injection level, neurons modeled with Nav1.2-L1342P had more action potential firing than neurons modeled with WT Nav1.2 channel. The input-output relationship, representing the number of action potentials elicited by the corresponding current input, showed that L1342P neurons had substantially more action potentials firing compared to WT over a broad range of current injections (**Figure 2B**). To evaluate single action potential waveform changes, phase plots were constructed from the first derivative of the membrane potential (dV/dt) versus the membrane potential (**Figure 2C**). We found a slightly lower action potential threshold in the L1342P neurons, with no detectable difference between WT and L1342P neurons in peak amplitude or maximum value of dV/dt. Collectively, our results from the computational modeling suggest an overall hyperexcitability phenotype in neurons carrying the Nav1.2-L1342P variant, which prompts us to test our hypothesis in human neuron-based models.

3. hiPSCs carrying L1342P variant can be differentiated into a cortical glutamatergic neuronal fate.

Excitatory glutamatergic neurons in the cortex are a key cell type involved in seizures (Howell *et al.*, 2015; Ben-Shalom *et al.*, 2017; Ogiwara *et al.*, 2018). The methodology to reliably generate cortical glutamatergic neurons is well established (Deneault *et al.*, 2019; Ghatak *et al.*, 2019; Quraishi *et al.*, 2019). To understand how the heterozygous Nav1.2-L1342P variant affects the function of human cortical neurons, we used CRISPR/Cas9 to recapitulate the sequence change of heterozygous Nav1.2-L1342P in a human reference iPSC line (Skarnes *et al.*, 2019) (referred to L1342P thereafter). The Nav1.2-L1342P variant has been identified from multiple patients with shared as well as distinct phenotypes (Matalon *et al.*, 2014; Dimassi *et al.*, 2016; Li *et al.*, 2016; Wolff *et al.*, 2017) (Hackenberg *et al.*, 2014). Thus, a reference hiPSC line had the advantage to reduce the influence of the genetic background across individual patients, and allowed us to assess the impact of the Nav1.2-L1342P variant on neurons compared to isogenic controls.

After CRISPR/Cas9 mediated editing process, we successfully obtained both isogenic WT and heterozygous L1342P hiPSCs validated by sequencing (**Figure 3A**). Both isogenic WT and L1342P hiPSCs can be differentiated into cortical neurons using an established protocol (**Figure 3B**). Undifferentiated hiPSC colonies displayed normal and homogenous morphology with defined edges and low levels of spontaneous differentiation. They consistently express pluripotency markers, including SOX2 and TRA-1-80 (**Figure 3C**). When we differentiate these hiPSCs into neural progenitor cells, we identified high proportions of dorsal telencephalic neuroepithelial marker PAX6 and

FOXG1, both supporting the forebrain identity of these neural progenitor cells (**Figure 3D**). After 45 days of maturation, differentiated cortical neurons displayed a morphology with neurites, and expressed mature neuron-specific markers. Staining of microtubule-associated protein 2 (MAP2) was found to be mainly localized to both soma and dendritic compartments, and staining of βIII-tubulin+ was seen in the soma, dendrites, and extended processes (**Figure 3E-G**). Moreover, the vast majority of hiPSCs-derived cortical neurons express vesicular glutamate transporter 1 (VGLUT1), indicating an abundant presence of glutamatergic neurons (**Figure 3E**). To determine the structural maturity of neurons, presynaptic proteins synapsin 1 and 2 (SYN1/2) were studied, which were found to be distributed along the axons in dotted patterns, indicating the formation of connectivity (**Figure 3F**). Expression of cortical marker CTIP2 was also evident in culture, indicating cortical characteristics (**Figure 3G**). Together, these data provide evidence that the CRISPR-engineered hiPSCs carrying isogenic WT and Nav1.2-L1342P can be differentiated into cortical glutamatergic neurons.

4. Human iPSC-derived cortical neurons carrying L1342P variant display intrinsic hyperexcitability

Our results from computational modeling and whole-cell voltage-clamp recordings suggested that the neurons carrying the Nav1.2-L1342P variant would display a gain-of-function phenotype. To test our hypothesis, we used cortical neurons derived from hiPSCs to exam the functional consequence of the Nav1.2-L1342P variant. After maturation for at least 45 days, pyramidal-shaped neurons were selected for whole-cell current-clamp experiments (**Figure 4A**). Neurons were held at a fixed –75 mV membrane potential to eliminate variation in resting membrane potential to assess the triggered firing. We progressively depolarized the neurons by intracellular current injections from 0 - 135 pA, with a step of 5 pA increment. We found that the isogenic WT neurons did not fire an action potential until the injected current reached 80 pA, which was defined as the rheobase. In contrast, the L1342P neuron started to fire with a lower current injection of 60 pA (**Figure 4B**). Quantitatively, we found a 25% reduction in rheobase of L1342P neurons, statistically different from isogenic WT neurons (**Figure 4C**) (WT: 78.7 ± 5.3 pA, n = 27; L1342P: 57.4 ± 4.3 pA, n = 31; p = 0.003, *student's t-test*). We further analyzed the voltage threshold of spiking, since it is likely to be influenced by sodium channel dysfunctions (Ye *et al.*, 2018). Our results revealed that L1342P neurons had a lower voltage threshold, which indicates a higher probability to fire under more hyperpolarized membrane potential (**Figure 4D**) (WT: –31.8 ± 1.5 mV, n = 27; L1342P: –36.3 ± 1.3 mV, n = 31; p = 0.02, *student's t-test*). Furthermore, we found that the amplitude of action potential was significantly enhanced in L1342P neurons, with an average amplitude approximately 7 mV larger than that of isogenic WT (**Figure 4E**) (WT: 20.1 ± 1.8 mV, n = 27; L1342P: 27.5 ± 1.9 mV, n = 31; p = 0.007, *student's t-test*). On the other hand, we found no statistical difference in spike width (**Figure 4F**) (WT: 4.9 ± 0.7, n = 27; L1342P: 3.7 ± 0.3, n = 31; p = 0.37, *student's t-test*) between the isogenic WT and L1342P neurons. These data indicate the L1342P variant makes the neurons easily to fire action potentials, rendering the neuron to be more excitable.

It was previously suggested that sodium channel variant may affect the trafficking or membrane expression of the channel to alter the channel density (Rusconi *et al.*, 2007; Thompson *et al.*, 2020) (Misra *et al.*, 2008). To elucidate whether the L1342P variant may

alter current density contributing to the increased excitability of the neurons, we recorded sodium current from our hiPSC-derived neurons in voltage-clamping mode. We were able to record a family of voltage-dependent inward current traces from the iPSC-derived neurons carrying WT as well as L1342P channel, with peak current nearly reaching 1 nA (**Figure 4G left**). After the application of phrixotoxin-3 (PTx-3, 10 nM), known to be a specific Nav1.2 channel blocker at or below 30 nM (Li *et al.*, 2014; Yin *et al.*, 2017; Risner *et al.*, 2020), the peak current was significantly reduced (**Figure 4G right**). Our data further validated that Nav1.2 current is one of the major components contributing to the total sodium current in these neurons, consistent with published literature (Ye *et al.*, 2018). When we compared the peak sodium current density between isogenic WT and L1342P neurons, we found a significantly greater sodium current density in L1342P neurons (**Figure 4H-I**) (WT: 85.5 ± 5.3 pF/pA, n = 18; L1342P: 122.9 ± 10.3 pF/pA, n = 21; p = 0.003, *student's t-test*). Higher current density of sodium channel, together with reduced rheobase and voltage threshold, thus is likely to serve as the basis underlying the increased intrinsic excitability of neurons carrying L1342P variant.

5. L1342P variant renders enhancement of repetitive firing in hiPSC-derived cortical neurons

To further investigate how the L1342P variant affects repetitive action potential firings, we performed whole-cell current clamp recording using a prolonged 400 ms current stimulus protocol. We injected a graded current stimulus to the neurons, and the number of action potential firings was recorded under each step of current injection during the range from 0 to 125 pA in 5 pA increment. Neurons carrying either WT or heterozygous L1342P generated repetitive action potentials spikes. From 45 to 55 pA stimulus, L1342P neuron fired 2-4 action potentials in response to current steps (**Figure 5A**). In contrast, single or at most two action potentials were elicited in isogenic WT neurons (**Figure 5A**)**.** Overall, the L1342P neurons fired significantly more action potentials than isogenic WT in the range of 0 - 125 pA (repeated-measures two-way ANOVA analysis, F (1, 39) = 6.67, p = 0.014) (**Figure 5B**)**.** It is worth noting that we also observed a distinct pattern from the input-output relationship of isogenic WT and L1342P neurons. Under depolarizing current within 0 - 20 pA, the firing frequency elicited between two groups in each step is similar. Starting from 20 pA, we observed a steeper slope of increase in firing from the L1342P neurons until 75 pA current injection, indicating that they are more responsive to stimulus during this range. However, the curve from L1342P neurons fell between the range of 75 - 125 pA, while isogenic WT neurons retained a similar spiking ability after achieving the plateau. Additionally, the maximum number of action potential firing that can be triggered by current injection was significantly different between isogenic WT and L1342P neurons, showing a 35% increase in L1342P neurons (**Figure 5C**) (WT: 3.4 ± 0.3, n = 18; L1342P: 4.6 ± 0.4, n = 23; *p* = 0.02, *student's t-test*). Together, our data suggest the L1342P variant greatly influenced the repetitive firing, leading to the hyperexcitability phenotype of neurons.

6. Neural network excitability is enhanced in neurons carrying the L1342P variant.

We have found elevated evoked action potential firing of individual neurons carrying the Nav1.2-L1342P variant in our patch-clamp recording. However, whether this enhanced intrinsic excitability translates into higher activities in a neural network is unknown. MEA is a relatively high-throughput extracellular recording assay that can

record the firing of a population of neurons in their normal culture medium (**Figure 6A**) (Yang *et al.*, 2018) (Yang *et al.*, 2016) (Mis *et al.*, 2019).

Spontaneous neuronal network activity was recorded from both isogenic WT and Nav1.2-L1342P variant in the absence of external stimulation in MEA (**Figure 6B**). The traces of a 2.5-sec epoch show that the L1342P neuron culture fired at a higher level than the isogenic WT culture (**Figure 6B**). The firing of a population of neurons can be visualized in a heat-map view, with each colored circle represent an active electrode (**Figure 6C**). The firing frequency is color-coded, with blue represents low firing frequency and yellow/red represents high firing frequency. In isogenic WT culture, two active electrodes exhibit low activity. On the other hand, a representative L1342P culture had five active electrodes with higher firing frequency (**Figure 6C**). Quantitatively, MEA recording confirmed that the mean firing frequency of L1342P culture is significantly higher, more than doubled compared with isogenic WT (**Figure 6D**) (WT: 0.31 ± 0.03 Hz, n = 19; L1342P: 0.70 ± 0.1 Hz, n = 17; P < 0.001, *student's t-test*). To further understand the temporal behavior of these neurons, we analyzed the raster plot, in which the recorded activity of each electrode was plotted over time. While we observed a similar number of active electrodes across wells, we detected more bursting events in the L1342P neuron culture compared to the isogenic WT culture (**Figure 6E**). In the isogenic WT culture, the active electrodes were firing at a relatively low frequency with scattered firing characteristics over 100 secs. In contrast, the representative well-wide raster plot of L1342P culture showed a higher firing rate over the 100-second recording window (**Figure 6E**).

Bursting events, including the bursting frequency, bursting duration, and bursting intensity (spiking frequency within each bursting event) were analyzed to further study the cultures' firing characteristics related to seizures (Fruscione *et al.*, 2018; Tukker *et al.*, 2018; Quraishi *et al.*, 2019; Tukker *et al.*, 2020a). The bursting frequency was significantly increased in the L1342P culture compared to isogenic WT (**Figure 6F**) (WT: 0.04 ± 0.009, n = 19; L1342P: 0.13 ± 0.02, n = 17; p = 0.0002, Mann-Whitney U). Interestingly, while the bursting duration was shortened significantly in L1342P culture (WT: 0.36 ± 0.02, n = 19; L1342P: 0.23 ± 0.01, n = 17; p < 0.0001, *student's t-test*) (**Figure 6G**), the bursting intensity was markedly elevated, which is reflected by the decreased inter-spike interval (ISI) within the burst (**Figure 6H**) (WT: 27 ± 1.1 Hz, n = 19; L1342P: 38 ± 2.0 Hz, n = 17; p < 0.0001, *student t-test*). Furthermore, we measured the synchrony index, which is determined by synchrony of spike firing between electrode pairs (Eggermont, 2006), to reflect the strength of synchronized activities between neurons (value is between 0-1, with 1 indicating the highest synchrony). The synchrony index was markedly increased in L1342P neuron culture by two times (**Figure 6I**), suggesting seizures-related synchronous firing (WT: 0.03 ± 0.01, n = 19; L1342P: 0.06 ± 0.006, n = 17; p = 0.04, Mann-Whitney *U*). These results are consistent with the observation of enhanced intrinsic excitability of L1342P neuron culture in patch-clamping recording, while further demonstrating elevated network excitability caused by the L1342P variant.

6. Cortical neurons carrying Nav1.2-L1342P variant have reduced sensitivity towards anticonvulsant phenytoin.

In clinical observations, patients carrying the Nav1.2-L1342P variant develop intractable seizures with a minimal response towards commonly used antiepileptic drugs

(Hackenberg *et al.*, 2014). To test if we could recapitulate the elements of this clinical observation in a cell-culture based model, we studied a commonly used first-line anticonvulsant phenytoin with our MEA platform. Phenytoin is known as a general sodium channel blocker, and has been shown to inhibit high-frequency repetitive spikings (Rogawski and Loscher, 2004) to control seizure episodes (Boerma *et al.*, 2016; Braakman *et al.*, 2017; Gorman and King, 2017; Gardella *et al.*, 2018). We found that in isogenic WT culture, 15 μM phenytoin started to reduce the mean firing rate, and a statistically significant reduction was reached with phenytoin at 30 μM (**Figure 6J**). However, 15 μM phenytoin did not reduce the mean firing rate of L1342P culture, and 40 μM of phenytoin was required to achieve a statistically significant reduction of mean firing rate in L1342P culture (**Figure 6K**), indicating that phenytoin is likely to be less effective in the L1342P culture. Our findings could suggest that neurons carrying the L1342P variant had a reduced sensitivity towards phenytoin, providing a plausible explanation for the clinical observation that patients carrying the Nav1.2-L1342P variant are largely resistant to the common therapies.

7. Nav1.2 specific inhibitor PTx-3 reduces spontaneous and KA-induced firing of neuronal culture with L1342P variant.

General sodium channel blockers (e.g., phenytoin) have limited efficacy for a number of patients with a variety of different sodium channel variants (Boerma *et al.*, 2016; Syrbe *et al.*, 2016; Braakman *et al.*, 2017; Wolff *et al.*, 2017). Therefore, the development of isoform-specific blockers to treat patients carrying a specific sodium channel variant in a precision medicine manner is desirable and is of great promise. Although Nav1.6 specific or Nav1.6/Nav1.2 dual blockers have been reported (Bialer *et al.*, 2018), isoform-specific blockers for Nav1.2 are not currently available. Neurotoxin phrixotoxin-3 (PTx-3) has been suggested as a Nav1.2 specific blocker when used at a dose at or below 30 nM (Li *et al.*, 2014; Yin *et al.*, 2017; Risner *et al.*, 2020). While PTx-3 may not be used in a clinical setting, to provide proof-of-concept evidence of the utility of Nav1.2 specific blocker for clinical translation, we studied the inhibitory effect of PTx-3 on our neuronal cultures.

We first tested the inhibition effect of PTx-3 on baseline neuronal firings. After adding the compound, the spikes from both groups were reduced markedly (**Figure 7A**). Quantitatively, our results suggested a highly effective reduction of baseline neuronal firing in both isogenic WT and L1342P cultures (**Figure 7B**) (WT: 0.41 ± 0.1, n = 6; p = 0.0008. L1342P: 0.38 ± 0.01, n = 6; p = 0.0009, one-way ANOVA, post hoc analysis with Bonferroni corrections, compared to the baseline). Next, we evaluated the potency of PTx-3 to inhibit neuron firings under the condition of a chemically induced hyperexcitable state to further model seizures. Kainic acid (KA, 5 μM), a glutamate receptor agonist, and a commonly used compound to chemically trigger epileptiform activities, was used (Odawara *et al.*, 2016; Taga *et al.*, 2019). After the addition of KA, we found the firings from both isogenic WT and L1342P culture were markedly enhanced (**Figured 7C top**). After the addition of PTx-3, we observed a strong reduction in the spike numbers (**Figure 7C bottom)**. Both mean firing frequency and bursting frequency were markedly reduced by PTx-3 in both isogenic WT and L1342P neuronal culture (**Figure 7D-E**) (MFF: WT: 0.31 ± 0.01, n=8, p <0.0001; L1342P: 0.20 ± 0.07, n = 6, p < 0.0001; bursting frequency: WT: 0.29 ± 0.1, n=8, p <0.0001; L1342P: 0.07 ± 0.06, n = 6, p < 0.0001; one-way ANOVA,

post hoc analysis with Bonferroni corrections, compared to the KA-induced activity). Interestingly, PTx-3 seems to have a slightly stronger inhibition effect on L1342P culture compared to those with isogenic WT culture (**Figure 7D-E**). Our results showed that the PTx-3 could effectively inhibit the firing of neuronal culture with L1342P variant, support the utility of an isoform-specific Nav1.2 blocker as a candidate for the development of novel anticonvulsant drugs.

Discussion

In this study, we characterized the biophysical properties of heterozygous Nav1.2-L1342P channel, and examined the intrinsic and network excitability of hiPSC-derived neurons carrying this variant. We revealed substantial and complex biophysical property changes in the L1342P variant. Our data predicted that these complex biophysical changes of the L1342P variant would result in an overall “gain-of-function” phenotype. Supporting this prediction, we found that cortical neurons derived from hiPSCs carrying heterozygous L1342P display enhanced sustainable action potential firings, larger spike amplitude, hyperpolarized firing threshold, lower rheobase, and greater sodium current density. By investigating the network activity of neuron populations using MEA, we revealed increased neural excitability with higher synchrony index in the L1342P culture compared to isogenic WT culture. Remarkably, we obtained evidence to show that hiPSCs-derived cortical neurons with L1342P variant are less sensitive to a commonly used anticonvulsant compound phenytoin but have equal or slightly stronger sensitivity to a Nav1.2 isoform-specific blocker.

Nav1.1, Nav1.2 and Nav1.6 are three major voltage-gated sodium channels expressing in the central nervous system (Trimmer and Rhodes, 2004), and variants in all these channels are associated with seizures. Nav1.1 is strongly expressed in the interneurons (Ogiwara *et al.*, 2007). Majority of the seizure-associated Nav1.1 variants are suggested to be loss-of-function, which could reduce the excitability of inhibitory interneurons, leading to less inhibition on principal excitatory neurons (Catterall *et al.*, 2010). In turn, without sufficient inhibition, these principal excitatory neurons become more excitable and promote seizures. On the other hand, both Nav1.2 and Nav1.6 are predominantly expressed in the principal excitatory neurons (Ye *et al.*, 2018). Epilepsy-associated Nav1.6 variants are suggested to be gain-of-function. Study found that these gain-of-function Nav1.6 mutations led to enhanced excitability of excitatory neurons derived from hiPSCs, which are suggested as the main mechanism underlying the Nav1.6 variant related seizure (Tidball *et al.*, 2020). Loss-of-function variants of Nav1.6 are also found in patients, but these patients do not have develop epileptic phenotypes (Gardella and Moller, 2019). The association between variants in Nav1.2 and seizure are more complicated. Intriguingly, seizures seem to be found in both gain-of-function and loss-of-function Nav1.2 variants (Wolff *et al.*, 2017; Wolff *et al.*, 2019). Because Nav1.2 is also expressed in the principal excitatory neurons, it is predicted that Nav1.2 variants would enhance neuronal excitability. However, this hypothesis has not been explicitly tested in human neurons. Here we showed that an epilepsy-associated Nav1.2 variant causes hyperexcitability and hypersynchronous firing in human excitatory neurons derived from iPSCs. To our knowledge, this paper is the first study demonstrating the functional consequence of an epilepsy-associated Nav1.2 variant in human neurons. We also

revealed that L1342P variant resulted in an increased window current and enhanced current density. The extra availability of Nav1.2 channels in the cell membrane, which possess altered biophysical properties to be easily open, is likely to push neurons into a hyperexcitable state promoting seizures. Indeed, various studies show correlated increased sodium current densities and gain-of-function phenotypes in the iPSC-derived neurons (Fruscione *et al.*, 2018; Ghatak *et al.*, 2019).

Interestingly, despite an overall gain-of-function phenotype associated with neuronal hyperexcitability, we also observed traits of loss-of-function, particularly in action potential firing. In the input-output relationship, we found the L1342P neurons initially responded to current stimulus increments similar to isogenic WT neurons, but failed to maintain sustainability in firing frequency at high current injection (**Figure 5B**). A similar converging trend of the input-output relationship was reported in a previously described mutation Q1478K in Nav1.1 (Cestele *et al.*, 2008). The Q1478K variant caused a "self-limiting" hyperexcitability phenotype, possibly caused by a significant reduction in sodium current density. However, we found an increased current density in L1342P, suggesting a different mechanism. Failure to maintain spiking could be a result of a high level of inactivation in L1342P neurons responding to a strong depolarizing stimulus, correlated with a substantially hyperpolarized fast-inactivation property. Further studies are needed to support this proposed mechanism.

A number of recently discovered variants in *SCN2A* from patients with childhood epilepsy also presented with evidence indicating developmental impairments (Miao *et al.*, 2020). The terminology of "developmental and/or epileptic encephalopathy" has been recently used to imply that the developmental impairments could occur independently of seizures (Maljevic *et al.*, 2017; Scheffer *et al.*, 2017). Indeed, profiling of patients with L1342P variant revealed developmental disorders (Hackenberg *et al.*, 2014; Matalon *et al.*, 2014; Dimassi *et al.*, 2016). Three out of five L1342P cases reported acquired microcephaly, brain volume loss, and reduced head circumference. Modeling these disease symptoms related to neurodevelopment still needs to be carefully investigated in the future.

Studies have traditionally used the heterologous expression system as a convenient platform to study ion channel variants related to epilepsies. This type of analysis is informative regarding the specific biophysical features of a particular variant (Ben-Shalom *et al.*, 2017; Berecki *et al.*, 2018; Mason *et al.*, 2019). Moreover, this biophysical analysis can also provide information regarding "the gain-of-function" versus the "loss-of-function" feature of that particular variant (Adney *et al.*, 2020) (Thompson *et al.*, 2020). Determining the gain versus loss-of-function is critically important, both for establishing genotype-phenotype correlations and for informing clinical practice. Indeed, an insightful clinical study has shown that seizures of patients carrying a traditionally "gain-of-function" Nav1.2 variant can be adequately controlled by sodium channel blockers, whereas this same class of sodium channel blockers exacerbate seizures and worsen outcomes for patients carrying a loss-of-function Nav1.2 variation (Wolff *et al.*, 2017; Wolff *et al.*, 2019). Using electrophysiology and human neurons derived from hiPSCs, here we provided evidence to show that neuron carrying Nav1.2-L1342P variant is clearly gain-of-function, despite complex biophysical properties revealed in the heterologous expression system.

Even with advanced genetic testing, controlling seizure is challenging in clinical practice. The standard antiepileptic drug (AED) guidelines are usually applied to patients indiscriminately (Wilmshurst *et al.*, 2015; Sanders *et al.*, 2018). A large percentage of patients thus may not benefit from the first antiepileptic drug that was prescribed to them and then have to go through a trial-and-error process with different drugs. This tedious and often ineffective process significantly increases the disease burden and may cause the optimal treatment window to be missed for children with epilepsy. Thus, there is a critical need to explore new approaches to guide clinical practice accounting for patients' genetic variations. In fact, even L1342P variant turns out to display a gain-of-function feature, common anticonvulsants still cannot control the seizures in patients carrying this variant. hiPSCs-based *in vitro* genetic models hold great promise to transform clinical practice. Neurons derived from hiPSCs are amenable for long-term studies and high-throughput parallel screening for targeted drug discovery. Pairing with MEA, a high-throughput, extracellular recording assay of neuronal activity (Odawara *et al.*, 2016) (Odawara *et al.*, 2018; Tukker *et al.*, 2020b), study has shown a successful application of patient-specific disease modeling to discover epilepsy therapies (Tidball *et al.*, 2020). Using the hiPSC-derived neurons, it was found that riluzole and phenytoin can target specific Nav1.6 variants to attenuate bursting phenotypes in vitro, and suppress patient seizure events in the clinical study (Tidball *et al.*, 2020). Here we showed that hiPSC-derived neurons carrying the drug-resistant Nav1.2-L1342P variant are not sensitive to phenytoin, but have equal or even stronger sensitivity towards an experimental isoform-specific Nav1.2 blocker. Our study demonstrates the usefulness of such a platform to potentially advance clinical practice, which warrants additional studies to streamline this process for future clinical translation.

In summary, we revealed a hyperexcitability phenotype in hiPSCs-derived cortical neurons carrying the L1342P variant. The variant displayed unique features in altering the neuronal excitability, revealing a possible pathogenic mechanism. Moreover, we demonstrated that our *in vitro* model is able to partially recapitulate the pharmaco-responsiveness of the Nav1.2-L1342P variant. Using this *in vitro* model, we further show, as a proof-of-principle, that isoform-specific Nav1.2 blocker may be an effective treatment of hyperexcitability caused by Nav1.2 gain-of-function variants. Our results highlight the utility of gene-edited, hiPSCs-derived neurons for mechanistic investigation of neurological disease-causing mutations, as well as a platform for drug discovery to advance personalized treatment for patients carrying a variety of genetic variants.

Methods:

1. Transfection of HEK293 cells with Nav1.2 plasmid.

The human embryonal kidney cells (tsA201 type) were cultured in Dulbecco's Modified Eagle Medium (DMEM) medium supplemented with 10% fetal bovine serum and 1% penicillin-streptomycin antibiotics. After reaching 80% confluency, cells were transiently transfected with Lipojet reagent (LipoJet™ In Vitro Transfection Kit, SignaGen Lab. Cat # SL100468) to introduce full-length human Nav1.2 cDNA WT or L1342P variant, which were constructed and fused with a GFP plasmid (gifts from Dr. Stephen Waxman, Yale University). After 24 hours, cells were dissociated into single cells using 0.25% trypsin (Corning, Cat # 25-053-CI) and plated on Poly-D-Lysine coated coverslips (Corning, Cat # 354086) for whole-cell patch-clamp recording.

2. CRISPR-Cas9 Editing of hiPSCs.

CRISPR-Cas9 editing of KOLF2-C1 iPS cells (p9) to generate Nav1.2-L1342P heterozygous single-cell derived clones was performed as described (Skarnes *et al.*, 2019). Briefly, cells were grown in a 5% CO_2/37°C incubator in StemFlex media (LifeTech) on Synthemax-treated wells (Synthemax II; Corning) and dissociated to single cells with Accutase (Stem Cell Technologies). In a volume of 0.1 ml Primary Cell Buffer (Lonza), 1.6 x 10^6 KOLF2-C1 cells were nucleofected (Lonza Amaxa 4D nucleofector; program CA137) with 20 mg Cas9 protein (HiFi; IDT), 16 mg single guide RNA (5'-ATCTATCATGAATGTACTTC; chemically-modified; Synthego), and 200 pmol of a 100-mer oligonucleotide repair template (5'- GTTGTAAATGCTCTTTTAGGAGCCATTCCATCTATCATGAATGTACTTCCGGTTTGTCTGATCTTTTGGCTAATATTCAGTATCATGGGAGTGAATCTCT; desalted Ultramer; IDT) containing the L1342P single nucleotide variant. Cas9 ribonucleoprotein complexes were assembled *in vitro* for 30 minutes prior to nucleofection. The cells were plated onto one well of a Synthemax-treated 6-well plate and in StemFlex media containing 1XRevitaCell (LifeTech), 30 mM HDR Enhancer (IDT), and cultured at 32°C (cold shock) for two days. After 24 hours, the media was changed to remove Revitacell. At 48 hours, the media was changed to StemFlex without HDR Enhancer and cultured to confluence at 37°C. Following the cloning of single-cell derived colonies, genomic DNA was isolated. The target region containing the L1342P SNV was amplified by PCR (0.6 kb amplicon; forward primer, 5'-GGAATTTGATCCCCAAGTGGTCTCT; reverse primer, 5'- AATGAGAGCTTTGCACTCACTGTAG) and subjected to Sanger sequencing (sequencing primer, 5'-TTGGAGCTACCAGAGTCTAG).

3. Generation of iPSC-derived neurons.

We generated our matured neurons using 3-4 individual differentiations with up to four different hiPSC lines (2 for each genotype) to minimize the probability that the phenotype was coming from the intra-cell line difference. We adopted a Dual-SMAD inhibition-based method, which is simultaneous inhibition of both Activin/Nodal and Bone Morphogenetic Protein (BMP) signaling pathway with small molecules, with modifications (Shi *et al.*, 2012; Boissart *et al.*, 2013; Mehta *et al.*, 2018). In detail, hiPSCs were grown

on a Matrigel substrate (Corning, Cat # 354230) in StemFlex Medium (Gibco, Cat # A3349401) until 80-90% confluency at 37 ºC and 5% CO_2. Colonies were passaged with an EDTA-based dissociation solution, Versene (Thermofisher, Cat # 15040066), and seeded with 10 mM rock inhibitor (RevitaCell Supplement, Gibco, Cat # A2644501) for the initial 24 hours on ultra-low attachment 96-well plates (Corning, Cat # CLS3474-24EA) with a cell density of 12,000 cells per well to obtain evenly shaped spherical embryoid bodies (EB). EBs were generated in an EB formation medium containing neural induction medium (Stemcell Technology, Cat # 05835) supplemented with 100 nM LDN-193189 (Sigma, Cat # SML0559) and 10 µM SB431542 (Tocris, Cat # 1614). After seven days, EBs were harvested and replated into rosettes to generate neural progenitor cells (NPCs). A neural rosette selection reagent (Stem Cell Technologies, Cat # #05832) was used to lift the rosette monolayer and allow expansion to obtain NPCs. Once neural progenitors were formed, they were plated on Poly-L-Ornithine (PLO)-laminin-coated coverslips and differentiated for the first seven days with a formula containing: neurobasal medium (Gibco, Cat #21103049), 1X B27 plus supplement (Gibco, Cat # A3582801), 1X Non-Essential Amino Acids Solution (NEAA; Gibco, Cat # 11140050), Glutamax (Gibco, Cat # 3505006). Then we switched the medium into maturation medium and continued culturing for the next 38 days containing: Brainphys (Stemcell Technology, Cat # 05790), 1X B27 plus supplement (Gibco, Cat # A3582801), 1X MEM Non-Essential Amino Acids Solution (NEAA; Gibco, Cat # 11140050), Glutamax (Gibco, Cat # 3505006), 100 µM Cyclic adenosine monophosphate (cAMP) (Santa Cruz Biotechnology, Cat # sc-201567A), 200 µM ascorbic acid, 10 ng/ml brain-derived neurotrophic factor (BDNF) (ProspecBio, Cat # CYT-207) and 10 ng/mL glial cell-derived neurotrophic factor (GDNF) (ProspecBio, Cat # CYT-305). Cell medium was replaced every 2-3 days.

4. Immunocytochemistry.

Immunocytochemistry was used to characterize the hiPSCs and determine the fate and maturity of differentiated neurons. The steps are described as follows: cells were maintained on glass coverslips (Neuvitro, Cat # GG-12-Pre) or 24 well glass bottom plates with #1.5 cover glass (Celvis, Cat #P24-1.5H-N) previously coated with PLO-Laminin. On the day of experiment, cells were washed briefly in phosphate-buffered saline (PBS 1X; Corning, Cat # 21-040-CMX12) and fixed in 4% paraformaldehyde in PBS at room temperature for 15 minutes. Samples were rinsed with PBS (5 minutes three times) and permeabilized for 20 minutes with 0.3% Triton-X (pH 7.4). Blocking steps were done with 5% Bovine Serum Albumin (BSA; Sigma Cat # 9048) for 1 hour, then left to incubate overnight with diluted primary antibodies in 1% BSA in a humidified chamber at 4°C. The following day, cells were washed three times with PBS and subjected to fluorescent-dye conjugated Alexa-Fluor based secondary antibodies diluted in 1% BSA for two hours at room temperature in the dark. After incubation, the secondary antibody solution was removed, and coverslips were washed three times with PBS for 5 min in the dark. For DAPI counterstain, VECTASHIELD® Antifade Mounting Medium with DAPI (Vector Laboratories Cat # H-1200) or a PBS-DAPI solution (Thermofisher, Cat# 62238) (1:10000) was used.

For neural progenitors: mouse- anti Paired box protein Pax-6 (PAX6) (Invitrogen, Cat #21103049) (1:300) and rabbit-anti Forkhead Box G1 (FOXG1) (Abcam, Cat # ab18259) (1:300) was used. For hiPSC-derived neurons: the primary antibodies were

rabbit-anti Anti-beta Tubulin III (Abcam, Cat # ab18207) (1:1000), mouse-anti Microtubule-associated protein 2 (MAP2) (Invitrogen, Cat # 13-1500) (1:1000), guinea pig-anti Synapsin1/2 (Synaptic Systems, Cat # 106044) (1:1000), rabbit-anti VGLUT1 (Synaptic Systems, Cat # 135 302) (1:1000) and CTIP2 (Abcam, Cat # ab18465) (1:300). Secondaries were anti-rabbit or mouse conjugated with Alexa-488 or Alexa-555, anti-guinea pig Alexa-488 and anti-rat Alexa-647 (Invitrogen) (1:1000). hiPSCs and neuronal cell imaging were acquired with a Widefield Nikon Eclipse Ti2 microscope. Images were processed and quantified using Nikon Imaging Software Elements. Representative Z-stack images for NPCs were acquired on a Nikon A1RMP inverted confocal.

5. Computational modeling on a cortical pyramidal cell model.

Computational modeling was used to predict the excitability reflected by neuronal spiking changes. The numerical simulations were run under the NEURON environment (Version 7.72, http://neuron.yale.edu) with a previously established model (Schmidt-Hieber and Bischofberger, 2010). The kinetic parameters of Nav1.2 were modified using a previously reported method according to activation and inactivation variables derived from our experimental data (Ben-Shalom *et al.*, 2017). Other parameters, including neuron physics and ion channel distribution, were in accordance with the literature (Schmidt-Hieber and Bischofberger, 2010) (Ben-Shalom *et al.*, 2017). To model the gating kinetics of the L1342P variant, the activation was set to vShift = -6. The number of spikes was counted during the 20 ms injection time. The phase plots were generated using the first single action potential waveform triggered and were superimposed for comparison.

6. Electrophysiology.

Whole-cell voltage-clamp recordings were performed with EPC10 amplifier and Patchmaster v2X90.3 software (HEKA Elektronik, Germany) coupled to an inverted microscope (NikonTi-2 Eclipse). Experiments were conducted at room temperature with 2–4 MΩ borosilicate glass pipettes. The extracellular voltage-clamping solution contained the following: 140 mM NaCl, 3 mM KCl, 1 mM CaCl2, 1 mM MgCl2, 10 mM HEPES, and 20 mM dextrose. The pipette solution contained the following: 140 mM CsF, 10mM NaCl, 1.1 mM EGTA, 10 mM HEPES, and 20 mM dextrose, then titrated with CsOH to pH 7.3. The osmolarity was adjusted with dextrose to 320 mOsm for the extracellular solution and 310 mOsm for the pipette solution. Leak currents were subtracted by the P/N procedure. Fast sodium currents were obtained by 10 ms voltage steps from − 80 mV to + 50 mV with 5mV increment, from a holding potential of − 100 mV. The trace was first fit with Boltzmann IV (Origin, version 9.7) to obtain the Vrev, then sodium conductance was calculated as GNa = INa / (Vm − Vrev), where INa is the peak current amplitude at Vm. For steady-state inactivation analysis, the value was determined using 500 ms prepulse to potentials from -140 to -5 mV, followed by a depolarizing test pulse to +5 mV. The window current was calculated as a percentage ratio between the overlapping area and the total area (over the range between -70 and 0 mV), under the activation and inactivation curves.

For current-clamp recording, 4-8 MΩ borosilicate glass pipettes were pulled, and the same recording system was used. The extracellular patch solution contained 140 mM NaCl, 3 mM KCl, 2 mM CaCl2, 2 mM MgCl2, 10 mM HEPES, 15 mM dextrose, and

internal solution contained 140 mM KCl, 3 mM Mg-ATP, 0.5 mM EGTA, 5 mM HEPES, and 20 mM dextrose. Dextrose was added to bring osmolarity to 320 mOsm and 310 mOsm, for the extracellular and internal solution, respectively. The pH value was titrated with KOH to pH 7.3. After the cells were matured for 50 days, 2-3 differentiated neurons from one dish were used for electrophysiological experiments. The pyramidal-shaped neurons with multipolar dendrites were selected for electrophysiological recording to ensure consistent neuron sampling. Action potential properties were analyzed from the first triggered AP in response to a depolarizing step. Rheobase was determined by the minimum current stimulus that can trigger the first action potential. The voltage threshold of the spiking waveform was determined at the voltage where a drastic upstroke is observed. The amplitude of action potential was measured from the peak to -75 mV. The spike width was determined by measuring the width of the action potential when the potential reaches half of the maximum amplitude. The current densities were obtained by normalizing the peak currents to the capacitance.

7. Micro-electrode-array (MEA) recordings on hiPSC-derived neurons

Neurons carrying both the Nav1.2-WT and heterozygous Nav1.2-L1342P were derived from the same protocol used for the patch-clamping experiment (2-3 individual preparations from each genotype). After 20 days of maturation, neuronal populations were dissociated into single cells using Accutase, and 100,000 cells in 10 µL suspension were plated on a pre-coated (Poly-L-Ornithine) 48-well plate Cytoview plates (Axion, Cat# m768-tMEA-48W) compatible with a Maestro MEA system (Axion Biosystems), with each well containing 16 electrodes. Cells were maintained in Brainphys (Stemcell Technology, Catalog #05790) medium supplemented with 100 µM cAMP, 10 ng/ml BDNF, 10 ng/ml GDNF, 200 µM ascorbic acid, and 1X B27 incubated in 37ºC for 14 days, with half-volume medium changes 2-3 times per week. On the day of recording, MEA plates with neurons were stabilized for 5 minutes in the system (Maestro, Axion Biosystems) at 5% of CO2 and 37ºC. A total of 200 seconds of recording time was used for analysis. The threshold for determining the voltage spikes was set greater than six standard deviations from background noise. Active electrodes were defined as >5 spikes per minute of recording, and wells with less than 25% active electrodes were not included in data analysis. The spike waveforms were continuously monitored to ensure the electrodes were intact and functioning correctly. Synchrony index, bursting frequency, bursting duration, and bursting intensity analysis were performed using the manufacturer software (Neural Metrics Tool, version 2.4. Axion Biosystems). The network synchrony between channels was measured based on the synchrony of spike firing between electrode pairs throughout the whole well (Eggermont, 2006). A burst was defined as a collection of at minimum five spikes, each separated by an inter-spike interval (ISI) of less than 100 ms.

The drug-testing was performed using the same 48-well plate during the culture time between 45-55 days. The plate was placed on the MEA system for 5 minutes, followed by a 100s recording to obtain the baseline measurement. After this, drugs were added to the MEA in a sterile condition, which will be followed by another 5-minute equilibrium. Then a 100s-long recording was made to study the drug effect. Fold changes were calculated by comparing the compound treatment to baseline (for phenytoin and PTx-3 baseline inhibition) or to KA (for PTx-3 inhibition on KA-induced firing). Drugs used in this study were: Kainic acid monohydrate (Sigma-Aldrich, Cat # K0250. 5 µM);

Phrixotoxin-3 (PTx-3) (R&D Systems, Cat # 4914. 15 μM); Phenytoin (Sigma-Aldrich, Cat # PHR1139. 15, 30, 40, 50 μM). KA and PTx-3 were freshly prepared in water. Stock solutions of phenytoin were made in DMSO (DMSO vehicle alone was used as the control, final concentration < 0.2%).

8. Statistical analysis and criteria for neuron selection

Data were analyzed using a parametric t-test, a nonparametric Mann-Whitney U test (If data is not normally distributed), or a repeated-measures one-way or two-way ANOVA on Origin (OriginLab Corp., Northampton, MA, USA) and Prism (GraphPad Software, Inc.). Data are reported as mean ± error (SEM). The significance threshold was set with a p-value less than 0.05 deemed as having a significant difference: $p \leq 0.05$ (*), $p \leq 0.01$ (**), and $p \leq 0.0001$ (***).

Figure 1

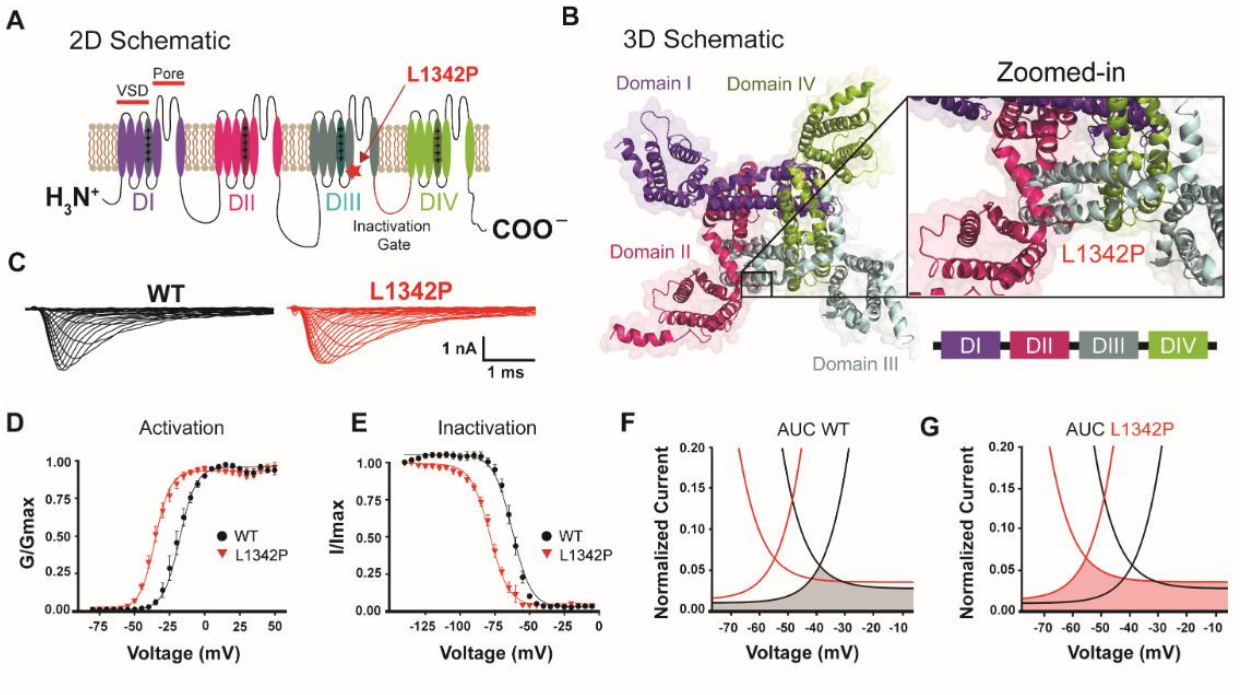

Figure 1. Structural location and biophysical properties of L1342P variant A. Schematic transmembrane topology of Nav1.2 sodium channel. Mutated residue L1342P is located at domain III, fifth segment, and is denoted as a red star. **B**. Cytosolic view of the structural model of Nav1.2 channel transmembrane domains. The location of L1342P variant is at the part of the pore-forming segment. A zoomed-in view was shown on the right. **C**. Representative traces for whole-cell sodium current from HEK cells expressing wild-type Nav1.2 (left) or Nav1.2-L1342P channel (right). **D.** Voltage-dependent activation. The normalized conductance was plotted against the voltages in the test pulse, ranging from –75mV to 50 mV, then fitted with the Boltzmann equation. **E.** Steady-state fast inactivation of wild-type and L1342P mutant channels. The relationship between the normalized current peak amplitude and prepulse potential was plotted and fitted with the Boltzmann function. **F-G**. Illustrative presentation of window current analysis for WT (**F**) and L1342P (**G**). The shaded area depicts window current, which is the overlapping region under activation and inactivation curves.

Figure 2

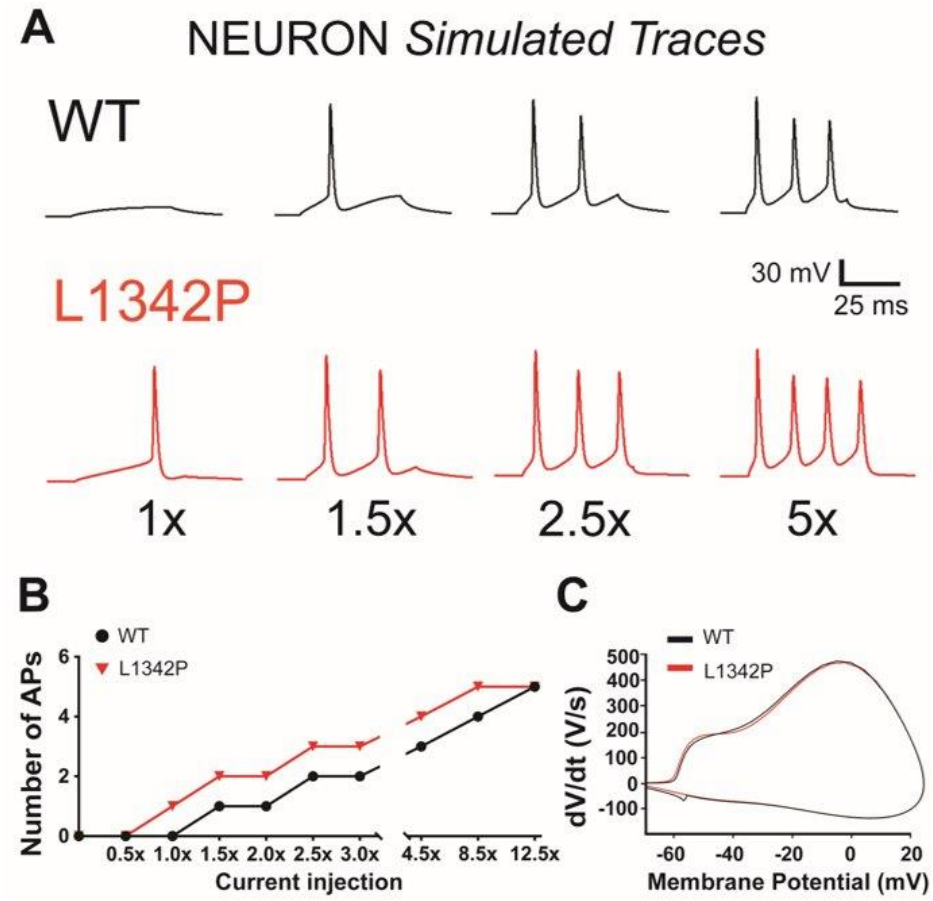

Figure 2. Single-compartmental simulation predicates gain-of-function in virtual neuron with Nav1.2-L1342P variant. A. Computational simulation predicated a higher firing frequency in the virtual neuron model with L1342P variant. **B.** Input-output relationship shows a significantly increased number of spikes in the range of current injections. **C.** Phase plot comparison between virtual WT and L1342P neuron. The virtual L1342P neuron has a slightly hyperpolarized voltage threshold, while no significant difference in other parameters.

Figure 3

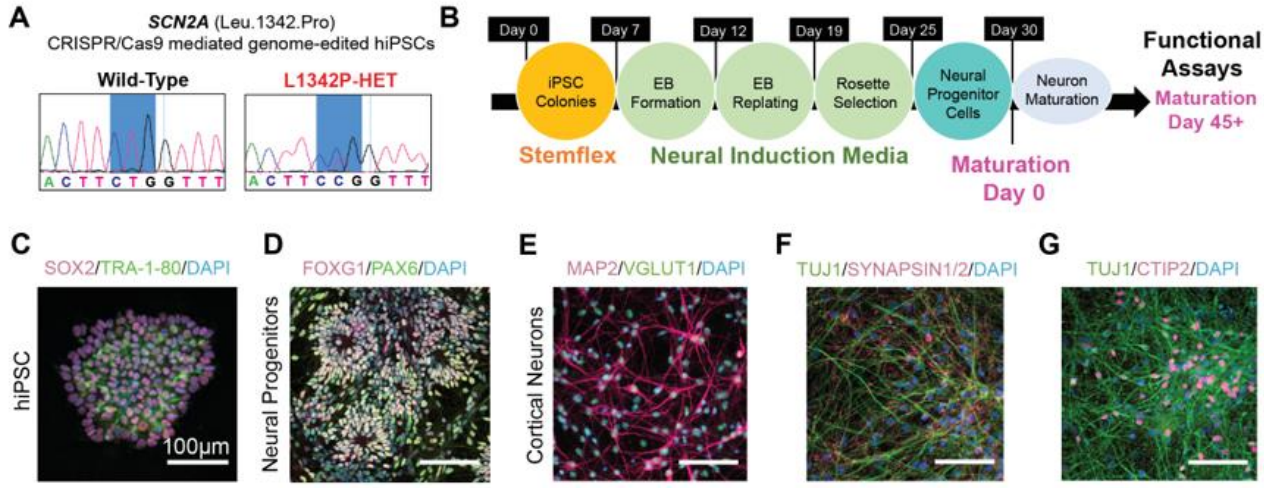

Figure 3. Characterization of hiPSC-derived neurons reveals a cortical neuron fate.

A. Sequencing of isogenic WT (black) and Nav1.2-L1342P variants (red) of iPSCs after CRISPR/Cas9 mediated genome-editing. **B.** Schematic of a modified DUAL-SMAD differentiation protocol and the timeline for experiments. **C.** Immunofluorescence staining of WT hiPSC with pluripotency markers SOX2 and TRA-1-80. **D.** Staining of neural progenitors with markers including FOXG1 and PAX6 (dorsal forebrain markers). **E.** Immunofluorescence image of WT hiPSC-derived glutamatergic neurons expressing MAP2, colocalized with VGLUT1. **F.** Culture formed connectivity between neurons, having colocalized expression of TUJ1 and synapsin1/2. **G.** Cortical layer marker CTIP2 indicates cortical identity of hiPSCs derived neurons. DAPI was used to stain nuclei.

Figure 4

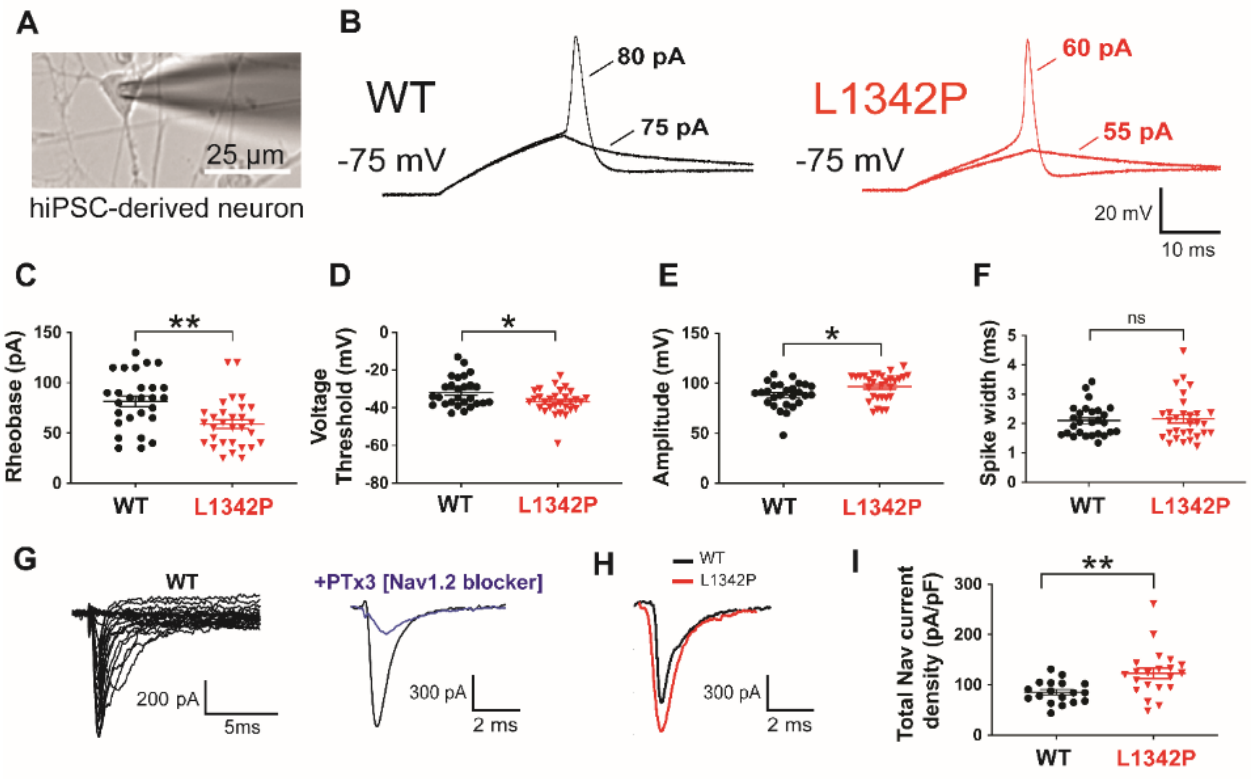

Figure 4. L1342P variant increases intrinsic excitability of cortical neurons derived from hiPSCs. A. hiPSCs derived pyramidal-shaped neuron selected for patch under the microscope. **B.** Representative single AP triggered by a stepwise increment of current stimulus, showing the difference in the rheobase of firing between isogenic WT and L1342P neurons at –75 mV holding potential. The current threshold was 80 pA for isogenic WT neuron, and 60 pA for L1342P neuron. **C.** The L1342P variant reduced the minimal current needed for evoking an action potential. **D**. Voltage threshold of action potential is hyperpolarized in L1342P neurons. **E**. Action potential from neurons carrying L1342P variant has elevated peak amplitude. **F**. The L1342P variant did not change the width of the action potential. **G**. Representative voltage-dependent sodium current traces (from isogenic WT neuron, left panel), with amplitude reduction after addition of PTx-3 (10 nM, right panel). **H**. Representative sodium current comparison between isogenic WT and L1342P neurons. Traces were plotted under –20 mV depolarizing step. **I**. Peak sodium current density reveals a significant increment in L1342P neuron. Data were collected from 4 independent differentiated batches with two clones used from each genotype. Data were analyzed with a *student's t-test*. * $p < 0.05$; ** $p < 0.01$.

Figure 5

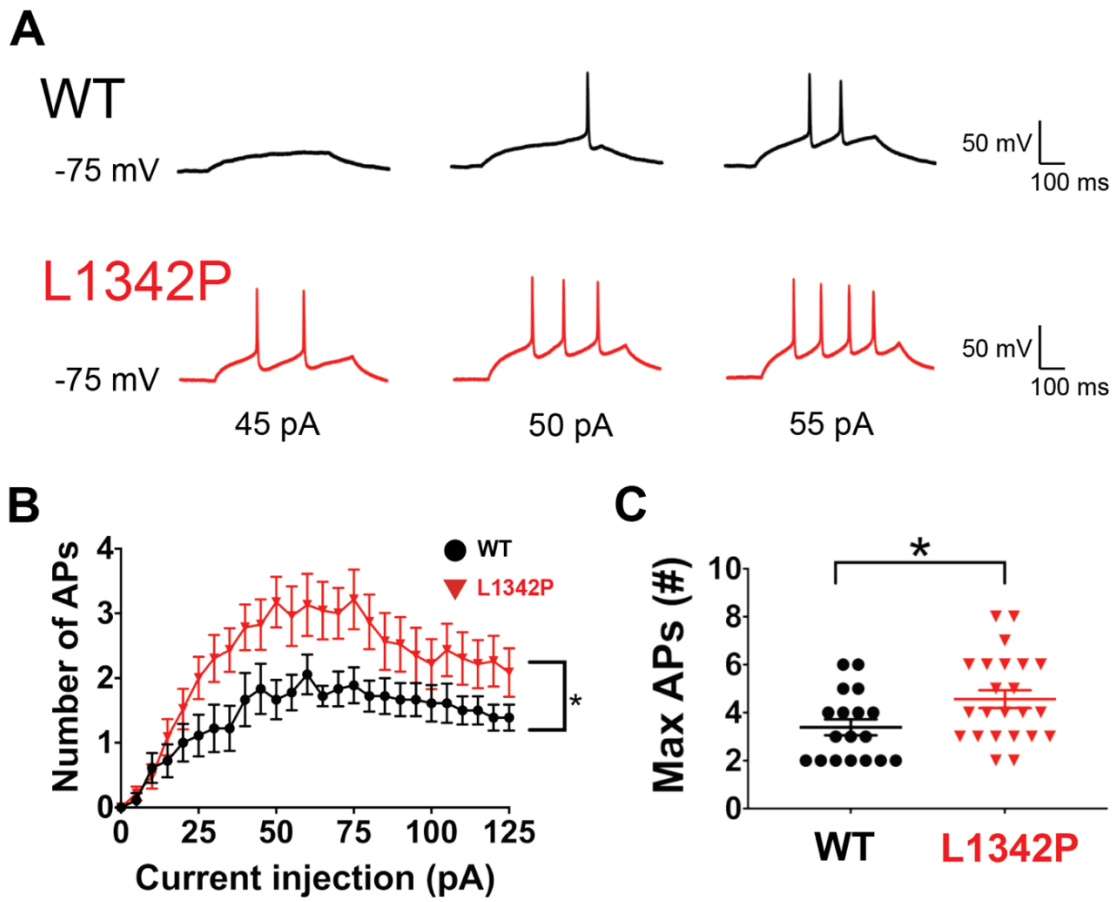

Figure 5. Repetitive firing is enhanced in neurons with the L1342P variant. A. Representative sustained action potential firings from hiPSC-derived cortical neurons expressing isogenic WT (black) and L1342P (red) mutated Nav1.2. **B.** Number of action potential (AP) firings in response to graded inputs from 0 to 125 pA current injection is shown. L1342P neurons constantly fire more action potentials than isogenic WT neurons . **C.** Maximum number of APs triggered from each neuron under the range of 0-125 pA current injections. Data were collected from 4 independent differentiated batches, with two clones used from each genotype. Data were analyzed by *student's t-test* * $p < 0.05$; ** $p < 0.01$.

Figure 6

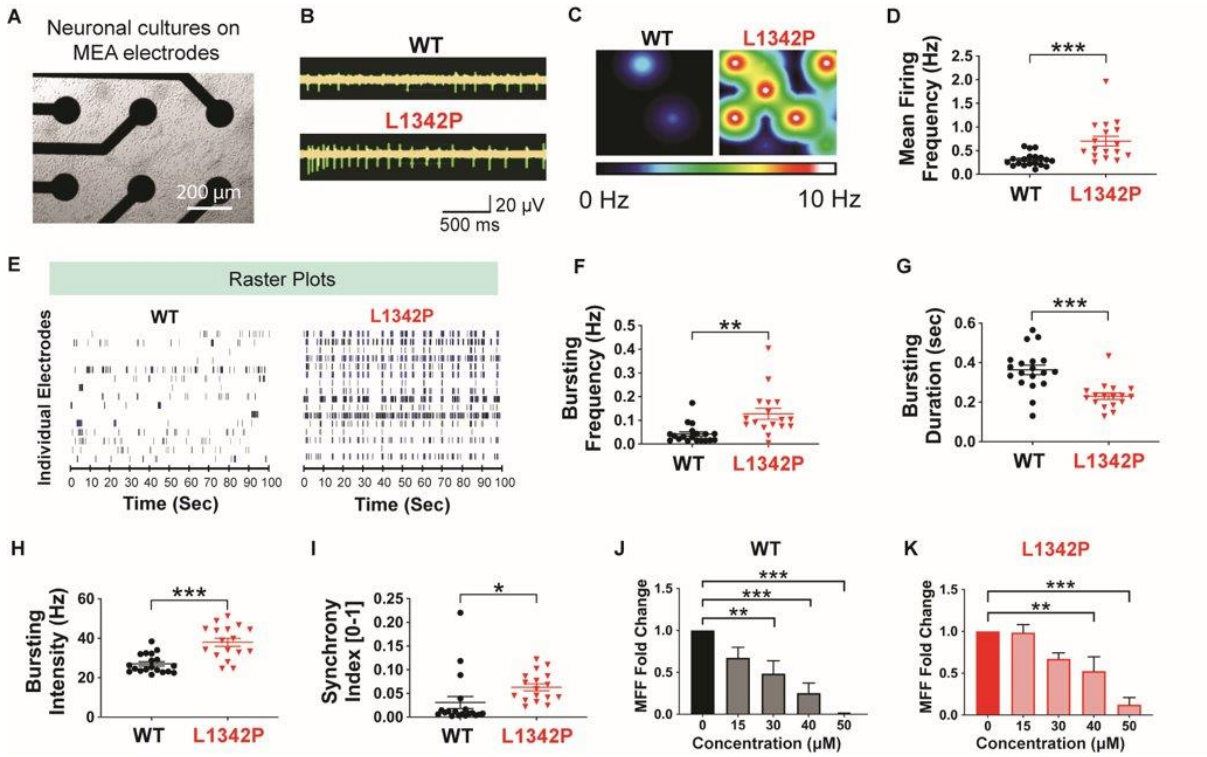

Figure 6. Micro-electrode array (MEA) recording of the firing of hiPSC-derived cortical neurons expressing WT and L1342P mutated channels. A. MEA well plated with hiPSC-derived neurons. **B.** Representative raw spikes from isogenic WT and L1342P cultures. Each spike indicates a spontaneous activity. **C.** Heat-maps recordings of neuronal firing. The intensity of firing frequency is color-coded, with warm colors (white, red, orange, and yellow) indicating high firing frequency and cool colors (green and blue) depicting low firing frequency. Each color circle represents an active electrode. **D.** Mean firing frequency (MFF) comparison between isogenic WT and L1342P culture. **E.** Representative spike raster plots from isogenic WT or Nav1.2-L1342P culture. Each row represents the spikes recorded from one electrode through 100 seconds, with each tick indicating one spontaneous event. Bursting events are depicted by a cluster of ticks. **F-I.** Parameters quantitatively describe the network activities in neuron culture including bursting frequency (F), bursting duration (G), and bursting intensity (H), Synchrony Index (I). Data are pooled from wells across four iPSC lines (2 for each genotype), with n=19 (wells) for isogenic WT and n=17 (wells) for the L1342P culture. The *student's t-test* was performed when data is normally distributed (Kolmogorov-Smirnov Normality Test), and Mann-Whitney U was performed when data is not normally distributed. * $p < 0.05$; ** $p < 0.01$. **J-K.** Inhibitory effects of different dosages of phenytoin between isogenic WT (J) and L1342P cultures (K). Data is presented as fold change of mean firing frequency of activities in response to increasing concentrations of phenytoin from 15-50 µM. The sample size was n=7, 8, 6, 6 (wells) for different concentration in WT culture, and n=6, 6, 6, 8 (wells) for L1342P culture. One-way ANOVA was performed, with Bonferroni corrections compared to the well before adding the drug. P-value is set at $p^* \leq 0.05$ (*), $p \leq 0.01$ (**), and $p \leq 0.0001$ (***).

Figure 7

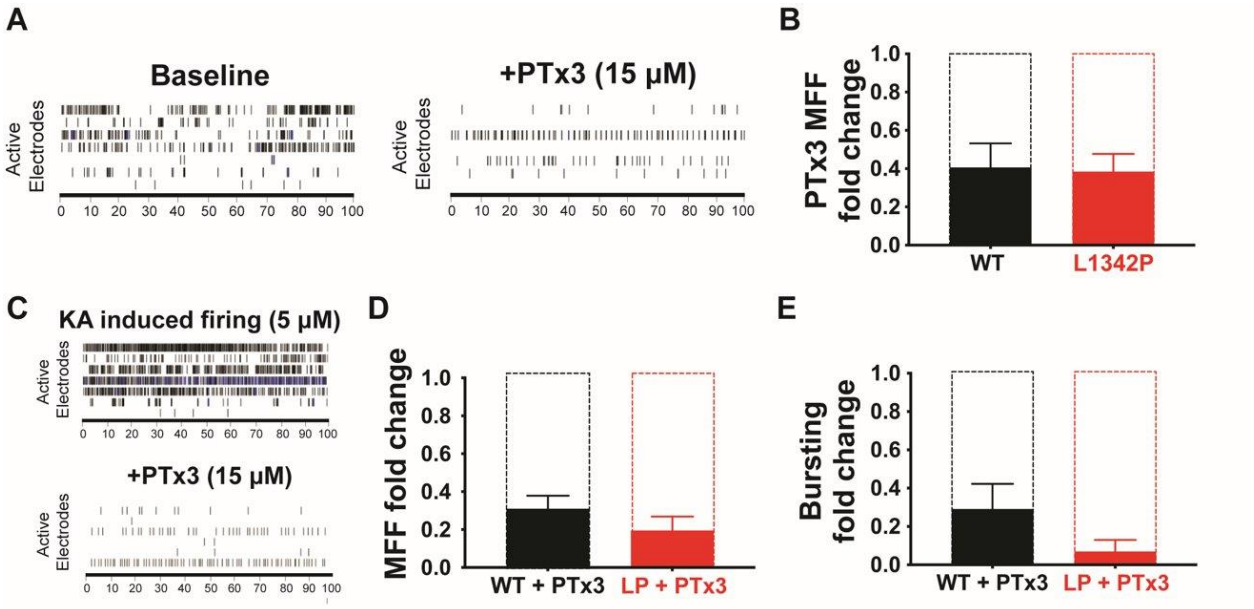

Figure 7. Phrixotoxin-3 (PTx-3) effectively suppressed spontaneous and KA-induced firings in L1342P culture. A. MEA recording shows that baseline mean firing frequency is reduced after the addition of PTx-3 in L1342P culture. **B.** Quantification of PTx-3 efficacy in inhibiting the baseline firing in both isogenic WT and L1342P culture. One-way *ANOVA* was performed, with Bonferroni corrections compared to the well before adding the drug. **C**. KA enhances neuronal firing by elevating the bursting, which can be effectively inhibited by PTx-3. **D.** Quantification of Ptx-3 efficacy in inhibiting the mean firing frequency in neuron culture after KA-stimulation. **E.** Quantification of PTx-3 efficacy in inhibiting the bursting firing activities in neuron culture after KA-stimulation. For baseline firing reduction analysis, n=6 (wells) for WT, and n=5 (wells) for L1342P culture. For inhibiting the KA-induced firing using the PTx-3, n= 8 (wells) for WT, and n=6 (wells) for L1342P culture. One-way *ANOVA* was performed, with Bonferroni corrections compared to the well with KA. P-value is set at $p^* \leq 0.05$ (*), $p \leq 0.01$ (**), and $p \leq 0.0001$ (***).

References:

Adney SK, Millichap JJ, DeKeyser JM, Abramova T, Thompson CH, George AL, Jr. Functional and pharmacological evaluation of a novel SCN2A variant linked to early-onset epilepsy. Annals of clinical and translational neurology 2020; 7(9): 1488-501.

Begemann A, Acuña MA, Zweier M, Vincent M, Steindl K, Bachmann-Gagescu R*, et al.* Further corroboration of distinct functional features in SCN2A variants causing intellectual disability or epileptic phenotypes. Molecular Medicine 2019; 25(1): 6.

Ben-Shalom R, Keeshen CM, Berrios KN, An JY, Sanders SJ, Bender KJ. Opposing Effects on NaV1.2 Function Underlie Differences Between SCN2A Variants Observed in Individuals With Autism Spectrum Disorder or Infantile Seizures. Biol Psychiatry 2017; 82(3): 224-32.

Berecki G, Howell KB, Deerasooriya YH, Cilio MR, Oliva MK, Kaplan D*, et al.* Dynamic action potential clamp predicts functional separation in mild familial and severe de novo forms of SCN2A epilepsy. Proc Natl Acad Sci U S A 2018; 115(24): E5516-E25.

Bialer M, Johannessen SI, Koepp MJ, Levy RH, Perucca E, Tomson T*, et al.* Progress report on new antiepileptic drugs: A summary of the Fourteenth Eilat Conference on New Antiepileptic Drugs and Devices (EILAT XIV). I. Drugs in preclinical and early clinical development. Epilepsia 2018; 59(10): 1811-41.

Boerma RS, Braun KP, van den Broek MP, van Berkestijn FM, Swinkels ME, Hagebeuk EO*, et al.* Remarkable Phenytoin Sensitivity in 4 Children with SCN8A-related Epilepsy: A Molecular Neuropharmacological Approach. Neurotherapeutics 2016; 13(1): 192-7.

Boissart C, Poulet A, Georges P, Darville H, Julita E, Delorme R*, et al.* Differentiation from human pluripotent stem cells of cortical neurons of the superficial layers amenable to psychiatric disease modeling and high-throughput drug screening. Transl Psychiatry 2013; 3: e294.

Braakman HM, Verhoeven JS, Erasmus CE, Haaxma CA, Willemsen MH, Schelhaas HJ. Phenytoin as a last-resort treatment in SCN8A encephalopathy. Epilepsia Open 2017; 2(3): 343-4.

Catterall WA, Kalume F, Oakley JC. NaV1.1 channels and epilepsy. J Physiol 2010; 588(Pt 11): 1849-59.

Cestele S, Scalmani P, Rusconi R, Terragni B, Franceschetti S, Mantegazza M. Self-limited hyperexcitability: functional effect of a familial hemiplegic migraine mutation of the Nav1.1 (SCN1A) Na+ channel. J Neurosci 2008; 28(29): 7273-83.

Deneault E, Faheem M, White SH, Rodrigues DC, Sun S, Wei W*, et al.* CNTN5(-)(/+)or EHMT2(-)(/+)human iPSC-derived neurons from individuals with autism develop hyperactive neuronal networks. Elife 2019; 8.

Dimassi S, Labalme A, Ville D, Calender A, Mignot C, Boutry-Kryza N*, et al.* Whole-exome sequencing improves the diagnosis yield in sporadic infantile spasm syndrome. Clin Genet 2016; 89(2): 198-204.

Eggermont JJ. Properties of correlated neural activity clusters in cat auditory cortex resemble those of neural assemblies. J Neurophysiol 2006; 96(2): 746-64.

Fruscione F, Valente P, Sterlini B, Romei A, Baldassari S, Fadda M*, et al.* PRRT2 controls neuronal excitability by negatively modulating Na+ channel 1.2/1.6 activity. Brain 2018; 141(4): 1000-16.

Gardella E, Marini C, Trivisano M, Fitzgerald MP, Alber M, Howell KB*, et al.* The phenotype of SCN8A developmental and epileptic encephalopathy. Neurology 2018; 91(12): e1112-e24.

Gardella E, Moller RS. Phenotypic and genetic spectrum of SCN8A-related disorders, treatment options, and outcomes. Epilepsia 2019; 60 Suppl 3: S77-S85.

Ghatak S, Dolatabadi N, Trudler D, Zhang X, Wu Y, Mohata M*, et al.* Mechanisms of hyperexcitability in Alzheimer's disease hiPSC-derived neurons and cerebral organoids vs isogenic controls. Elife 2019; 8.

Gorman KM, King MD. SCN2A p.Ala263Val Variant a Phenotype of Neonatal Seizures Followed by Paroxysmal Ataxia in Toddlers. Pediatr Neurol 2017; 67: 111-2.

Hackenberg A, Baumer A, Sticht H, Schmitt B, Kroell-Seger J, Wille D*, et al.* Infantile epileptic encephalopathy, transient choreoathetotic movements, and hypersomnia due to a De Novo missense mutation in the SCN2A gene. Neuropediatrics 2014; 45(4): 261-4.

Howell KB, McMahon JM, Carvill GL, Tambunan D, Mackay MT, Rodriguez-Casero V*, et al.* SCN2A encephalopathy: A major cause of epilepsy of infancy with migrating focal seizures. Neurology 2015; 85(11): 958-66.

Hu W, Tian C, Li T, Yang M, Hou H, Shu Y. Distinct contributions of Na(v)1.6 and Na(v)1.2 in action potential initiation and backpropagation. Nat Neurosci 2009; 12(8): 996-1002.

Jiruska P, de Curtis M, Jefferys JG, Schevon CA, Schiff SJ, Schindler K. Synchronization and desynchronization in epilepsy: controversies and hypotheses. J Physiol 2013; 591(4): 787-97.

Leha A, Moens N, Meleckyte R, Culley OJ, Gervasio MK, Kerz M*, et al.* A high-content platform to characterise human induced pluripotent stem cell lines. Methods 2016; 96: 85-96.

Li J, Cai T, Jiang Y, Chen H, He X, Chen C*, et al.* Genes with de novo mutations are shared by four neuropsychiatric disorders discovered from NPdenovo database. Mol Psychiatry 2016; 21(2): 298.

Li T, Tian C, Scalmani P, Frassoni C, Mantegazza M, Wang Y*, et al.* Action potential initiation in neocortical inhibitory interneurons. PLoS biology 2014; 12(9): e1001944.

Liao Y, Deprez L, Maljevic S, Pitsch J, Claes L, Hristova D*, et al.* Molecular correlates of age-dependent seizures in an inherited neonatal-infantile epilepsy. Brain 2010; 133(Pt 5): 1403-14.

Maljevic S, Reid CA, Petrou S. Models for discovery of targeted therapy in genetic epileptic encephalopathies. J Neurochem 2017; 143(1): 30-48.

Mason ER, Wu F, Patel RR, Xiao Y, Cannon SC, Cummins TR. Resurgent and Gating Pore Currents Induced by De Novo SCN2A Epilepsy Mutations. eNeuro 2019; 6(5).

Matalon D, Goldberg E, Medne L, Marsh ED. Confirming an expanded spectrum of SCN2A mutations: a case series. Epileptic Disord 2014; 16(1): 13-8.

Mehta SR, Tom CM, Wang Y, Bresee C, Rushton D, Mathkar PP*, et al.* Human Huntington's Disease iPSC-Derived Cortical Neurons Display Altered Transcriptomics, Morphology, and Maturation. Cell Rep 2018; 25(4): 1081-96 e6.

Miao P, Tang S, Ye J, Wang J, Lou Y, Zhang B*, et al.* Electrophysiological features: The next precise step for SCN2A developmental epileptic encephalopathy. Mol Genet Genomic Med 2020; 8(7): e1250.

Mis MA, Yang Y, Tanaka BS, Gomis-Perez C, Liu S, Dib-Hajj F*, et al.* Resilience to Pain: A Peripheral Component Identified Using Induced Pluripotent Stem Cells and Dynamic Clamp. The Journal of neuroscience : the official journal of the Society for Neuroscience 2019; 39(3): 382-92.

Misra SN, Kahlig KM, George AL, Jr. Impaired NaV1.2 function and reduced cell surface expression in benign familial neonatal-infantile seizures. Epilepsia 2008; 49(9): 1535-45.

Odawara A, Katoh H, Matsuda N, Suzuki I. Physiological maturation and drug responses of human induced pluripotent stem cell-derived cortical neuronal networks in long-term culture. Sci Rep 2016; 6: 26181.

Odawara A, Matsuda N, Ishibashi Y, Yokoi R, Suzuki I. Toxicological evaluation of convulsant and anticonvulsant drugs in human induced pluripotent stem cell-derived cortical neuronal networks using an MEA system. Sci Rep 2018; 8(1): 10416.

Ogiwara I, Miyamoto H, Morita N, Atapour N, Mazaki E, Inoue I*, et al.* Nav1.1 localizes to axons of parvalbumin-positive inhibitory interneurons: a circuit basis for epileptic seizures in mice carrying an Scn1a gene mutation. J Neurosci 2007; 27(22): 5903-14.

Ogiwara I, Miyamoto H, Tatsukawa T, Yamagata T, Nakayama T, Atapour N*, et al.* Nav1.2 haplodeficiency in excitatory neurons causes absence-like seizures in mice. Commun Biol 2018; 1.

Pan X, Li Z, Huang X, Huang G, Gao S, Shen H*, et al.* Molecular basis for pore blockade of human Na(+) channel Nav1.2 by the mu-conotoxin KIIIA. Science 2019; 363(6433): 1309-13.

Patlak J. Molecular kinetics of voltage-dependent Na+ channels. Physiol Rev 1991; 71(4): 1047-80.

Quraishi IH, Stern S, Mangan KP, Zhang Y, Ali SR, Mercier MR*, et al.* An Epilepsy-Associated KCNT1 Mutation Enhances Excitability of Human iPSC-Derived Neurons by Increasing Slack KNa Currents. The Journal of neuroscience : the official journal of the Society for Neuroscience 2019; 39(37): 7438-49.

Risner ML, McGrady NR, Pasini S, Lambert WS, Calkins DJ. Elevated ocular pressure reduces voltage-gated sodium channel NaV1.2 protein expression in retinal ganglion cell axons. Exp Eye Res 2020; 190: 107873.

Rogawski MA, Loscher W. The neurobiology of antiepileptic drugs. Nat Rev Neurosci 2004; 5(7): 553-64.

Rusconi R, Scalmani P, Cassulini RR, Giunti G, Gambardella A, Franceschetti S*, et al.* Modulatory proteins can rescue a trafficking defective epileptogenic Na(v)1.1 Na+ channel mutant. Journal of Neuroscience 2007; 27(41): 11037-46.

Rush AM, Dib-Hajj SD, Waxman SG. Electrophysiological properties of two axonal sodium channels, Nav1.2 and Nav1.6, expressed in mouse spinal sensory neurones. J Physiol 2005; 564(Pt 3): 803-15.

Sanders SJ, Campbell AJ, Cottrell JR, Moller RS, Wagner FF, Auldridge AL*, et al.* Progress in Understanding and Treating SCN2A-Mediated Disorders. Trends Neurosci 2018; 41(7): 442-56.

Scheffer IE, Berkovic S, Capovilla G, Connolly MB, French J, Guilhoto L*, et al.* ILAE classification of the epilepsies: Position paper of the ILAE Commission for Classification and Terminology. Epilepsia 2017; 58(4): 512-21.

Schmidt-Hieber C, Bischofberger J. Fast sodium channel gating supports localized and efficient axonal action potential initiation. J Neurosci 2010; 30(30): 10233-42.

Shi Y, Kirwan P, Smith J, Robinson HP, Livesey FJ. Human cerebral cortex development from pluripotent stem cells to functional excitatory synapses. Nat Neurosci 2012; 15(3): 477-86, S1.

Shorvon SD. The etiologic classification of epilepsy. Epilepsia 2011; 52(6): 1052-7.

Skarnes WC, Pellegrino E, McDonough JA. Improving homology-directed repair efficiency in human stem cells. Methods 2019; 164-165: 18-28.

Spratt PWE, Ben-Shalom R, Keeshen CM, Burke KJ, Jr., Clarkson RL, Sanders SJ*, et al.* The Autism-Associated Gene Scn2a Contributes to Dendritic Excitability and Synaptic Function in the Prefrontal Cortex. Neuron 2019; 103(4): 673-85 e5.

Streeter I, Harrison PW, Faulconbridge A, Flicek P, Parkinson H, Clarke L. The human-induced pluripotent stem cell initiative-data resources for cellular genetics. Nucleic acids research 2017; 45(D1): D691-D7.

Syrbe S, Zhorov BS, Bertsche A, Bernhard MK, Hornemann F, Mutze U*, et al.* Phenotypic Variability from Benign Infantile Epilepsy to Ohtahara Syndrome Associated with a Novel Mutation in SCN2A. Mol Syndromol 2016; 7(4): 182-8.

Taddese A, Bean BP. Subthreshold sodium current from rapidly inactivating sodium channels drives spontaneous firing of tuberomammillary neurons. Neuron 2002; 33(4): 587-600.

Taga A, Dastgheyb R, Habela C, Joseph J, Richard JP, Gross SK*, et al.* Role of Human-Induced Pluripotent Stem Cell-Derived Spinal Cord Astrocytes in the Functional Maturation of Motor Neurons in a Multielectrode Array System. Stem Cells Transl Med 2019; 8(12): 1272-85.

Thompson CH, Ben-Shalom R, Bender KJ, George AL. Alternative splicing potentiates dysfunction of early-onset epileptic encephalopathy SCN2A variants. The Journal of general physiology 2020; 152(3).

Tian C, Wang K, Ke W, Guo H, Shu Y. Molecular identity of axonal sodium channels in human cortical pyramidal cells. Front Cell Neurosci 2014; 8: 297.

Tidball AM, Lopez-Santiago LF, Yuan Y, Glenn TW, Margolis JL, Clayton Walker J*, et al.* Variant-specific changes in persistent or resurgent sodium current in SCN8A-related epilepsy patient-derived neurons. Brain 2020; 143(10): 3025-40.

Trimmer JS, Rhodes KJ. Localization of voltage-gated ion channels in mammalian brain. Annu Rev Physiol 2004; 66: 477-519.

Tukker AM, Van Kleef R, Wijnolts FMJ, De Groot A, Westerink RHS. Towards animal-free neurotoxicity screening: Applicability of hiPSC-derived neuronal models for in vitro seizure liability assessment. ALTEX 2020a; 37(1): 121-35.

Tukker AM, Wijnolts FMJ, de Groot A, Westerink RHS. Human iPSC-derived neuronal models for in vitro neurotoxicity assessment. Neurotoxicology 2018; 67: 215-25.

Tukker AM, Wijnolts FMJ, de Groot A, Westerink RHS. Applicability of hiPSC-Derived Neuronal Cocultures and Rodent Primary Cortical Cultures for In Vitro Seizure Liability Assessment. Toxicol Sci 2020b; 178(1): 71-87.

Wilmshurst JM, Gaillard WD, Vinayan KP, Tsuchida TN, Plouin P, Van Bogaert P*, et al.* Summary of recommendations for the management of infantile seizures: Task Force Report for the ILAE Commission of Pediatrics. Epilepsia 2015; 56(8): 1185-97.

Wolff M, Brunklaus A, Zuberi SM. Phenotypic spectrum and genetics of SCN2A-related disorders, treatment options, and outcomes in epilepsy and beyond. Epilepsia 2019; 60 Suppl 3: S59-S67.

Wolff M, Johannesen KM, Hedrich UBS, Masnada S, Rubboli G, Gardella E*, et al.* Genetic and phenotypic heterogeneity suggest therapeutic implications in SCN2A-related disorders. Brain : a journal of neurology 2017; 140(5): 1316-36.

Yang Y, Adi T, Effraim PR, Chen L, Dib-Hajj SD, Waxman SG. Reverse pharmacogenomics: carbamazepine normalizes activation and attenuates thermal hyperexcitability of sensory neurons due to Nav 1.7 mutation I234T. British journal of pharmacology 2018; 175(12): 2261-71.

Yang Y, Huang J, Mis MA, Estacion M, Macala L, Shah P*, et al.* Nav1.7-A1632G Mutation from a Family with Inherited Erythromelalgia: Enhanced Firing of Dorsal Root Ganglia Neurons Evoked by Thermal Stimuli. The Journal of neuroscience : the official journal of the Society for Neuroscience 2016; 36(28): 7511-22.

Ye M, Yang J, Tian C, Zhu Q, Yin L, Jiang S*, et al.* Differential roles of NaV1.2 and NaV1.6 in regulating neuronal excitability at febrile temperature and distinct contributions to febrile seizures. Sci Rep 2018; 8(1): 753.

Yin L, Rasch MJ, He Q, Wu S, Dou F, Shu Y. Selective Modulation of Axonal Sodium Channel Subtypes by 5-HT1A Receptor in Cortical Pyramidal Neuron. Cereb Cortex 2017; 27(1): 509-21.